Acta Cryst. (1997). A53, 314–328

Coincidence Lattices and Quasilattices for Icosahedral Quasicrystals

D. H. WARRINGTON,[a]* O. RADULESCU[b] AND R. LÜCK[c]

[a]*University of Sheffield, Department of Engineering Materials, Sheffield, England,* [b]*Laboratoire de Recherche sur les Matériaux, Université de Marne-la-Vallée, 2 rue de la Butte Verte, 93166 Noisy le Grand, France, and* [c]*Max-Planck-Institut für Metallforschung, Seestrasse 75, D-70174 Stuttgart, Germany. E-mail: d.warrington@sheffield.ac.uk*

(*Received 9 April 1996; accepted 24 December 1996*)

Abstract

The theory of CSL and DSC has been applied for grain boundaries of quasicrystals. Particular features of special grain boundaries of quasicrystals are underlined. The Frank–Rodrigues representation of rotations is used to classify disorientations and to find the degeneracy of different values of the coincidence index.

1. Introduction

Several intermetallics, in systems such as Al–Mn, Al–Cu–Fe, Al–Pd–Mn, show diffraction patterns with non-crystallographic point symmetry and Bragg peaks. This new type of long-range-ordered but aperiodic solids are called quasicrystals. Transmission electron microscopy used to investigate the diffraction phenomena also showed the existence of grain boundaries and twins. Thus, fundamental problems arise: what is the structure of a coherent interface between aperiodic but long-range-ordered structures; do the concepts of CSL (coincidence site lattice) and DSC (displacement shift complete lattice) have a meaning for quasicrystals and what are the particular features of twins in quasicrystals? This paper gives some answers to these questions and provides useful tools for further studies. We restrict ourselves to the case of the icosahedral quasicrystals, which are of most experimental interest.

It was shown (Warrington, 1993) that CSLs and DSCs (Ranganathan, 1966; Bollmann, 1970) can be applied to the crystallography of grain boundaries of quasicrystals.

A full understanding of the properties of planar and linear defects of icosahedral quasicrystals requires knowledge of their six-dimensional (6D) representation (Katz & Duneau, 1986). Thus, dislocation lines and their Burgers vectors are conveniently represented as 4D manifolds and 6D lattice vectors, respectively, in a 6D hypercubic crystal (Socolar, Lubensky & Steinhardt, 1986; Kléman, 1988). Similarly, grain boundaries in icosahedral quasicrystals can be represented as 5D interfaces in the 6D crystal (Radulescu, 1994). The matrices that describe the disorientation of the grains are 6D rotation matrices, the CSL and DSC are 6D lattices (Radulescu, 1994; Warrington & Lück, 1995; Radulescu & Warrington, 1995). According to this, and responding to requirements of experimental works, we provide the list of the 6×6 rotation matrices for all coincidence indices $\Sigma < 50$, together with the basis vectors of grain-boundary dislocations for $\Sigma \leq 11$.

The point symmetry of the grains multiplies the number of rotations that produce the same disorientation. Choosing a single representative in the family of all symmetry-related rotations is useful for experimental statistics of disorientations. For this purpose, we adopt a method proposed by Frank (1988) and we discuss some properties of what we call 'rotation tiles', the sets of rotations that are repeated by symmetry in rotation space.

A general introduction to N-dimensional CSL theory (Fortes, 1983) makes no mention of the important special conditions leading to CSLs in quasicrystals because it was written before the discovery of quasicrystals.

The present paper follows the presentation by the authors of arithmetic properties associated with directions and coincidences in quasicrystals (Radulescu & Warrington, 1995). Parallel and complementary work (Baake & Pleasants, 1995*a*,*b*); Pleasants, Baake & Roth, 1996; Baake, 1996) gives an algebraic solution to the derivation of CSL rotations.

2. Coincidences in quasicrystals

The icosahedral quasicrystal is a three-dimensional structure but it allows a simpler description in six dimensions. We can geometrically obtain the quasicrystal by a 'cut and project' procedure, applied to a 6D hypercubic crystal (Katz & Duneau, 1986).

A 3D tiling model of a primitive (P-type) icosahedral quasicrystal is similar to the unit-cell description of a periodic crystal, with the exception that for the quasicrystal one defines two rhombohedral tiles (an oblate and a prolate) with a volume ratio τ, and which recur in a quasiperiodic way. The edges of the tiles belong to a star of six vectors $\mathbf{e}_i^{\parallel}$, $i = 1,\ldots,6$, which point from the centre to the vertices of an icosahedron, and their relative directions are best shown on the stereographic projection (Fig. 1). This allows any vertex in the tiling to be indexed† with a set of six integer indices z_i, $i = 1,\ldots,6$, and to consider it as the projection of a vertex

† There are $384 = 2^6 6!/120$ non-equivalent ways of associating the $\mathbf{e}_i^{\parallel}$ with the six vectors; we use the particular choice of Kramer, Papadopoulos & Zeidler (1991).

of a 6D hypercubic lattice and any tile edge to be the projection of a unit 6D vector $\mathbf{e}_i$. The above indices refer to the direct space and, in contradistinction to the case of a lattice, they take only some of the possible integer values (because the tiling vertices project from a cut in the hyperlattice).

The interface between two rotated 3D tilings will (as for crystals) show a good fit if there are coincidences of the vertices of the disoriented tilings. These coincidences exist for special rotation matrices. As in Radulescu & Warrington (1995), we call the set of all coincidences in the tiling a coincidence quasilattice (CQL) and the special 3D rotations that produce coincidences quasirational rotations (Q-ROT).

The rotation matrix that produces a CSL for a 3D crystal has rational coefficients in a suitably chosen basis. There is no such 3D basis for a Q-ROT. In order to get a rational coefficients matrix for a Q-ROT, one must either extend the notion of rational numbers (Pleasants, Baake & Roth, 1996) or lift the action of the rotation to 6D (as we are doing subsequently). There is a simple way of constructing this 6D rational matrix. All we need are six independent coincidences, taken for instance from a drawing of the coincidences in the 3D tiling. Using the indexing scheme from above, we have six pairs of 6D integer vectors, which will define a 6D rational matrix $\mathbf{R}$ as follows: If $\mathbf{R}^{\parallel}$ is the 3D Q-ROT, then

$$\mathbf{R}^{\parallel} \sum_{j=1}^{6} x_{ij}\mathbf{e}_j^{\parallel} = \sum_{j=1}^{6} y_{ij}\mathbf{e}_j^{\parallel}, \quad i = 1, \ldots, 6,$$

where x_{ij} and y_{ij} are integers. However, since the edges of the tiles as seen in a 2D (see Figs. 2*a–d*) or 3D projection can be identified with the projections of the basis vectors in 6D,

$$\mathbf{R} = \mathbf{Y}\mathbf{X}^{-1}$$

with

$$\mathbf{X} = [x_{ij}]_{i,j=1,\ldots,6}, \quad \mathbf{Y} = [y_{ij}]_{i,j=1,\ldots,6}. \tag{1}$$

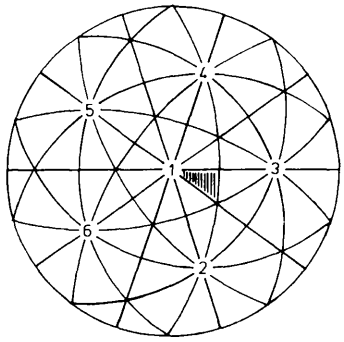

Fig. 1. Stereographic projection showing fivefold axes $\mathbf{e}_i^{\parallel}$, $i = 1, \ldots, 6$, and standard stereographic triangle.

As for 3D crystals, $\mathbf{R}$ can be written as

$$\mathbf{R} = (1/F)[R_{ij}]_{i,j=1,\ldots,6}, \tag{2}$$

where R_{ij} and F are coprime integers satisfying

$$\sum_{i=1}^{6} R_{ij}^2 = F^2. \tag{3}$$

Rotation matrices that satisfy (2) and (3) produce a 6D CSL in the 6D hypercubic lattice. We have therefore arrived at a condition for coincidences in a 6D lattice. The standard techniques (Grimmer, Bollmann & Warrington, 1974) for deriving a basis for the CSL and DSC lattices in 3D may be directly adapted for 6D. Nevertheless, not all solutions of (2) and (3) will have a meaning for icosahedral quasicrystals. Q-ROTs in 3D arise only from a restricted set of rotation matrices $\mathbf{R}$, which commute with the projector $\mathbf{\Pi}$ onto the physical space that carries the quasicrystal (otherwise $\mathbf{R}$ will destroy the quasicrystal geometry). Thus we have the additional condition:

$$\mathbf{R}\mathbf{\Pi} = \mathbf{\Pi}\mathbf{R}, \tag{4}$$

where

$$\mathbf{\Pi} = \tfrac{1}{2}\left(1 + \mathbf{S}/5^{1/2}\right) \tag{5}$$

and

$$\mathbf{S} = \begin{bmatrix} 0 & 1 & 1 & 1 & 1 & 1 \\ 1 & 0 & 1 & \bar{1} & \bar{1} & 1 \\ 1 & 1 & 0 & 1 & \bar{1} & \bar{1} \\ 1 & \bar{1} & 1 & 0 & 1 & \bar{1} \\ 1 & \bar{1} & \bar{1} & 1 & 0 & 1 \\ 1 & 1 & \bar{1} & \bar{1} & 1 & 0 \end{bmatrix} \tag{6}$$

Relation (4) implies that $\mathbf{R}$ block-diagonalizes into two 3D rotations: one is $\mathbf{R}^{\parallel}$, which acts in the physical space, and the other is $\mathbf{R}^{\perp}$, which acts in the orthogonal complement of the physical space (this 3D space is usually called perpendicular space):

$$\mathbf{A}\mathbf{R}\mathbf{A}^{-1} = \begin{bmatrix} \mathbf{R}^{\parallel} & \mathbf{0} \\ \mathbf{0} & \mathbf{R}^{\perp} \end{bmatrix}. \tag{7}$$

The rotation $\mathbf{A}$ that performs the block-diagonalization is the same for any $\mathbf{R}$:

$$\mathbf{A} = \frac{1}{[2(\tau+2)]^{1/2}} \begin{bmatrix} 1 & \bar{1} & 0 & \tau & \tau & 0 \\ \tau & \tau & 1 & 0 & 0 & 1 \\ 0 & 0 & \tau & 1 & \bar{1} & \bar{\tau} \\ \bar{\tau} & \tau & 0 & 1 & 1 & 0 \\ 1 & 1 & \bar{\tau} & 0 & 0 & \bar{\tau} \\ 0 & 0 & 1 & \bar{\tau} & \tau & \bar{1} \end{bmatrix}, \tag{8}$$

where $\tau = (1 + 5^{1/2})/2$ is the golden ratio. The column vectors of the upper and the lower 3×6 matrices are the 3D vectors $\mathbf{e}_i^{\parallel}$ and $\mathbf{e}_i^{\perp}$, respectively, the physical and the perpendicular components of the 6D unit vectors.

Also, the physical and perpendicular components of an arbitrary hyperlattice vector $\mathbf{r}$ are, respectively,

$$\mathbf{r}^{\parallel} = \mathbf{\Pi}\mathbf{r} \quad \text{and} \quad \mathbf{r}^{\perp} = (\mathbf{1} - \mathbf{\Pi})\mathbf{r}. \tag{9}$$

It follows that the lengths of $\mathbf{r}^{\parallel}$ and $\mathbf{r}^{\perp}$ are given by

$$\begin{aligned} |\mathbf{r}^{\parallel}| &= [(\mathbf{r}\cdot\mathbf{r}5^{1/2} + \mathbf{r}\cdot\mathbf{S}\mathbf{r})/(2\times 5^{1/2})]^{1/2}, \\ |\mathbf{r}^{\perp}| &= [(\mathbf{r}\cdot\mathbf{r}5^{1/2} - \mathbf{r}\cdot\mathbf{S}\mathbf{r})/(2\times 5^{1/2})]^{1/2}. \end{aligned} \tag{10}$$

This relationship is particularly useful to find the perpendicular component of DSC vectors (§8). Also, the rotations $\mathbf{R}^{\parallel}$ and $\mathbf{R}^{\perp}$ defined above are one to one related, their rotation axes being the physical and perpendicular component, respectively, of the same hyperlattice vector $\mathbf{d}$, and their rotation angles satisfy

$$\begin{aligned} \cos(\varphi^{\parallel}) &= \tfrac{1}{4}[\mathrm{Tr}(\mathbf{R}) + \mathrm{Tr}(\mathbf{RS})/5^{1/2} - 2] \\ \cos(\varphi^{\perp}) &= \tfrac{1}{4}[\mathrm{Tr}(\mathbf{R}) - \mathrm{Tr}(\mathbf{RS})/5^{1/2} - 2] \end{aligned} \tag{11}$$

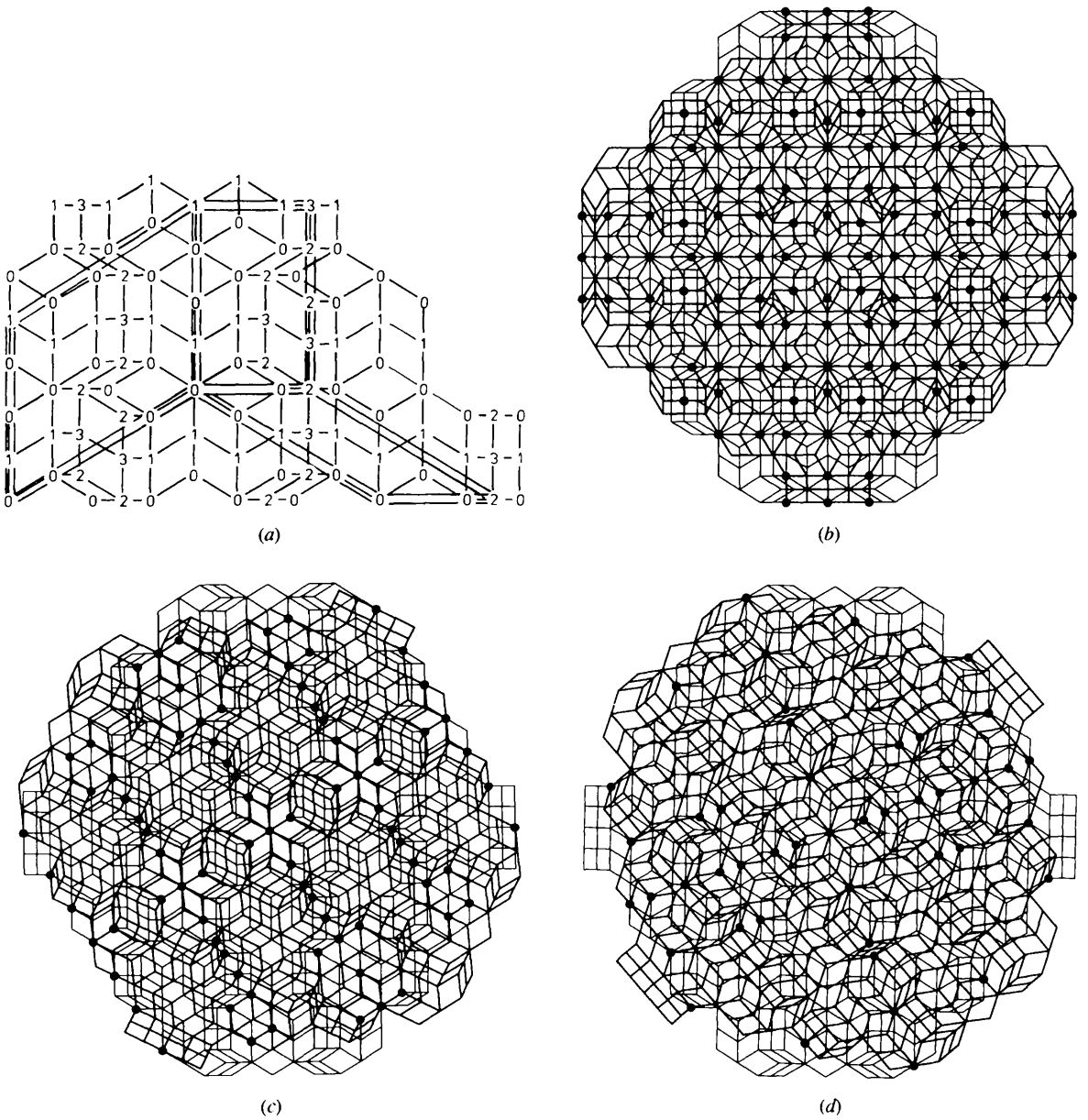

(*a*) (*b*) (*c*) (*d*)

Fig. 2. Coincidences in a twofold Wieringa roof obtained by cut and projection (according to Katz & Duneau, 1986). (*a*) The labelling shows the succession of four different heights but does not imply equal height increments. The roof (with heights on) has inflation symmetry (vertices occur in existing positions when the pattern is scaled by τ^3). Note the different distributions in cases (*b*) $\Sigma 4$, (*c*) $\Sigma 5$, (*d*) $\Sigma 9$. $\Sigma 4$ (*b*) contains false coincidences (different heights, same 2D projection) that do not belong to the 3D CQL; we did not mark these with dots.

3. The Wieringa roof, its advantages and disadvantages

The lozenge faces of the rhombohedra that compose the icosahedral Penrose tiling have all the geometry of a face of a regular triacontahedron and are the projections of 2D square faces of the 6D hypercube. As first proposed by Katz & Duneau (1986), the 3D tiling may be displayed by use of a Wieringa roof (de Bruijn, 1981), which consists of a connected set of faces of the rhombohedra lying between two planes normal to a chosen axis, no hidden faces being present when one looks along this axis. These roofs have corrugated appearance and do not contain all the tiling vertices within the slice between the two planes. Viewed along the normal axis, the roof appears as a planar pattern of a number of different tiles that match one with another. To each vertex of the planar tiling may be ascribed a 'height' of the vertex in the roof, which is measured along the normal axis. These heights can be easily derived from the 6D indices $\{r_i\}_{i=1,\ldots,6}$ of the vertices and the 6D indices $\{d_i\}_{i=1,\ldots,6}$ of the axis orthogonal to the roof and are proportional to $p + q \times 5^{1/2}$, where $p = \sum_{i,j=1}^{6} r_i S_{ij} d_j$ and $q = \sum_{i=1}^{6} r_i d_i$. A simplified presentation of these heights and a discussion of characteristic scaling properties of the patterns can be found in Warrington & Lück (1995).

The restrictions imposed on the Wieringa roofs are rather loose and leave some arbitrariness in the choice of the roof inside a given slice. Nevertheless, for rotated undisplaced quasicrystals, the roof orthogonal to the rotation axis possesses the remarkable property of showing, when heights are taken into consideration, a value of the coincidence ratio that is close to that in 6D. For this reason, roofs and heights were the raw data for the first determination of coincidence rotations (Warrington, 1993; Warrington & Lück, 1995). On the other hand, a relative displacement of the quasicrystals may lead to a reduction in the number of coincident vertices appearing in the roof, which is not representative of the situation in 6D. This effect will be discussed more fully in §8, where it will be shown how it may be corrected.

4. Coincidence ratio and index

We equate a coincidence index Σ for the 6D CSL to the ratio of the volumes of primitive unit cells of the CSL and the hyperlattice. We define an effective coincidence ratio Σ_e as the inverse density of coincident vertices for the coincidence quasilattice CQL in the 3D tiling (or in general in any quasilattice). Σ is well defined and can be derived from the matrix $\mathbf{R}$ by the same techniques as for 3D matrices. One can show that for icosahedral quasicrystals Σ takes positive values of the form $5x^2 - y^2$, x, y integers (Radulescu, 1994, 1995) or, which is the same thing, of the form $p^2 + pq - q^2$ (Baake & Pleasants, 1995*a*,*b*). Σ_e depends on both $\mathbf{R}$ and the relationship between the tiling and the hyperlattice. The standard way to obtain a quasiperiodic tiling is to select those points of the hyperlattice, included in a band, and to project them onto the physical space. The band is parallel to the 3D physical space and its intersection $\mathcal{A}$ with the 3D perpendicular space is called the acceptance domain. The CQL is the projection onto the physical space of points of the 6D CSL included in a band parallel to the physical space and whose intersection with the perpendicular space is the domain $\mathcal{D}$ common to $\mathcal{A}$ and $\mathbf{R}^\perp\mathcal{A}$ (*i.e.* $\mathcal{D} = \mathcal{A} \cap \mathbf{R}^\perp\mathcal{A}$). As the volumes $V(\mathcal{A})$ of $\mathcal{A}$ and $V(\mathcal{D})$ of $\mathcal{D}$ are generally different, a correction factor must be applied (Radulescu, 1994; Radulescu & Warrington, 1995) in order to get Σ_e:

$$\Sigma_e = [V(\mathcal{A})/V(\mathcal{D})]\Sigma. \tag{12}$$

$V(\mathcal{D})$ is maximized and close to $V(\mathcal{A})$ (Σ_e being minimized and close to Σ), when the symmetry centre of $\mathcal{A}$ is on the rotation axis of $\mathbf{R}^\perp$. Any translation of $\mathcal{A}$ from this position increases Σ_e (see also §8). Equation (12) and the fact that the acceptance domain $\mathcal{A}$ is not spherical* implies that Σ_e is always greater than Σ for a non-defective tiling.

5. The set of coincidence rotations or quasirational rotations (Q-ROT)

The experimentalist requires a list of disorientations (the smallest angle equivalent rotation *via* the symmetry of the grains) for the smallest values of Σ that are experimentally accessible.

Several approaches may be used. The first one is restricted to low values of Σ by a visual investigation of the tilings of Wieringa roofs (Warrington, 1993; Warrington & Lück, 1995). Another searching technique surpasses the earlier technique in speed and accuracy by looking for coincidences in the rank 6 module that contains the tiling. Although six independent coincidences are needed to determine a 6D matrix $\mathbf{R}$, only three non-coplanar coincidences suffice since three more may be obtained by applying to them the generalized inflation matrix $\mathbf{S}$, which commutes with $\mathbf{R}$ and with the projector $\mathbf{\Pi}$ (Radulescu, 1994). Baake & Pleasants (1995*a*,*b*) have developed an algebraic technique based on icosians. Development of the technique of Warrington & Buffalini (1971), which searches for diophantine solutions to the columns of the rotation matrices, is inefficient and lacks further insight into the problem.

We use here another route with a geometrical foundation, which is that any Q-ROT is equivalent either to a 180° rotation about a quasicrystalline direction (twin axis, see Appendix *A*), or to a product of two such 180° rotations (which for two axes at Φ apart in a plane P is a

* For icosahedral quasicrystalline tilings, $\mathcal{A}$ is a regular triacontahedron, a polyhedron with 30 rhombic faces.

rotation of 2Φ about an axis normal to P). An analytical formula gives the value of Σ for a 180° rotation as a function of the 6D indices of the rotation axis (see Appendix *A*). We list in Table 1 all twin axes within the unit stereographic triangle that correspond to values of Σ less than an arbitrarily chosen value (here 50). Values of Σ for products of 180° rotations about these axes or about those equivalent to them can be computed by standard matrix manipulation, and we thus select other rotation axes of Q-ROT (not of 180°) with $\Sigma < 50$. We put all the axes (the 180° rotation axes and the others) in Table 2 in order of decreasing density. The numbering of the axes in this table has no universal meaning but depends on our choice to include all axes used for $\Sigma < 50$ (using higher values of Σ would introduce further axes and require a different ordering of those present). The convention used for the 6D indexing of the axes is given in Appendix *A*. The values of Σ, together with the disorientation rotation matrices, the axes and the values of the angles for the set of symmetry-equivalent rotations, are given in Table 1.

5.1. *Degeneracy of the values of* Σ

There exist several Q-ROTs that produce the same coincidence index. The first type of this degeneracy can be explained by the symmetry of the quasicrystal.

Let us call two rotations $\mathbf{R}_1$, $\mathbf{R}_2$ equivalent if

$$\mathbf{R}_1 = \mathbf{S}_1\mathbf{R}_2\mathbf{S}_2, \tag{13}$$

where $\mathbf{S}_1, \mathbf{S}_2$ are symmetry rotations of the quasicrystal.

Two equivalent rotations produce the same disorientation and the same coincidence index. If in the above definition $\mathbf{S}_1 = \mathbf{S}_2^{-1}$, then the two rotations are conjugate and have the same angles and axes of the same crystallographic form. Two rotations may be equivalent, without being conjugate (they may have non-equivalent rotation axes or different angles). In addition to (13), $\mathbf{R}_1$ is inversely equivalent to $\mathbf{R}_2$ if it is equivalent to $\mathbf{R}_2^{-1}$. If this is the case, then $\mathbf{R}_1$ acting on the first grain produces the same disorientation as $\mathbf{R}_2$ acting on the second grain. A geometrical method to determine the number of equivalent and inversely equivalent rotations will be presented in §6.

A second type of degeneracy of the value of the coincidence index occurs when rotations are related by a symmetry of the hyperlattice but not by a symmetry of the quasicrystal.† This type of degeneracy has been discussed (Radulescu, 1994; Radulescu & Warrington, 1995) and when it exists is always twofold (disorientations related by such a symmetry are marked with an asterisk in Table 1, for instance $\Sigma 11$ and $\Sigma 11^*$). Finally, a third type of degeneracy has no symmetry connotation (an example in Table 1 is given by the disorientations $\Sigma 31_1$, $\Sigma 31_2$), which is also known in 3D cubic crystals and arises from different diophantine solutions of equations (3).

† The complete point symmetry group of the hypercubic lattice is $\Omega(6)$, the hyperoctahedral group, which contains as a subgroup Y_h the point symmetry group of the quasilattice.

6. The disorientation tile and Frank–Rodrigues space

One may define a rotation space in which any rotation $\mathbf{R}$ is represented by a vector parallel to the rotation axis with a length determined by the rotation angle. For icosahedral symmetry, this space may be divided into tetrahedral tiles, each tile containing rotations that are not symmetry related; the purpose is to reduce (by symmetry combinations $\mathbf{S}_1\mathbf{R}\mathbf{S}_2$ or $\mathbf{S}_1\mathbf{R}^{-1}\mathbf{S}_2$) an experimentally determined rotation $\mathbf{R}$ to a standard disorientation description.

Frank (1988) discussed the utility of various representations of rotations as vectors in a 3D space and showed that the Rodrigues mapping, which associates a vector $\mathbf{n}\tan(\omega/2)$ in a 3D space [called hereafter Frank–Rodrigues (F–R) space] to a rotation of angle ω and axis $\mathbf{n}$, has two useful properties. These are that planes and lines in the F–R space transform to planes and lines on pre- or post-rotations by any arbitrary rotation, and that the locus of all rotations, equally misoriented from two reference rotations, is a plane orthogonal to the difference vector between the reference rotations.

The second property allowed Frank to divide F–R space into polyhedral cells, similar to the Voronoi decomposition of the direct space of a crystal lattice or to the Brillouin-zone decomposition of the reciprocal space. The cells are centred on symmetry rotation vectors. For the group Y, there are 60 such cells; that containing the origin of the F–R space is a pentagonal dodecahedron, containing the smallest angle descriptions (disorientations) of rotations, and called by Frank the fundamental zone. The highly symmetric vertices on the border of the fundamental zone are all low-coincidence Σ Q-ROT [maximum angles of 36° ($\Sigma 5$), 41.81° ($\Sigma 9$) and 44.48° ($\Sigma 4$), on fivefold, twofold and threefold axes, respectively].

The fundamental zone may be subdivided into 120 tetrahedral tiles, with vertices of $\Sigma 1$, $\Sigma 4$, $\Sigma 5$ and $\Sigma 9$. This avoids two equivalent or inversely equivalent rotations within the same tile. The tile corresponding to the unit stereographic triangle is called the standard disorientation tile. The other cells may be correspondingly subdivided, see Fig. 3.

One interest in this construction is to reduce a given rotation to one within the standard disorientation tile. Tables 1 and 2 facilitate this operation. For example, a Q-ROT of 63.43° about a twofold axis (no. [1] in Table 2) is found in line 2 of Table 1 to be equivalent to a 36° standard disorientation about a fivefold axis (no. [2]).

F–R construction also reveals some rules for the distribution of Q-ROTs in the space of all rotations.

Table 1. *Q-ROT and sets of equivalent rotations with axes in the unit stereographic triangle (UST rotations) for* $\Sigma < 50$

Rotations are given by their 6D matrices, or are represented as $(\varphi^{\parallel}, \varphi^{\perp})[d]$, where $\varphi^{\parallel}$, $\varphi^{\perp}$ are the rotation angles in the physical and perpendicular space, respectively, and d is the rotation axis.

Σ	$\mathbf{R}\times F$						F	Disorientation	Equivalent UST rotations
4	0	1	1	0	1	1	2	(44.48, 164.48)[3]	(44.48, 164.48)[3](75.52, 75.52)[3](90.00, 90.00)[1]
	1	0	1	−1	−1	0			(110.21, 154.76)[8](138.59, 138.59)[11](154.76, 110.21)[7]
	1	1	0	1	0	−1			(164.48, 44.48)[3](180.00, 180.00)[4]
	1	−1	0	1	0	1			
	1	0	−1	−1	1	0			
	0	1	−1	0	−1	1			
5	5	0	0	0	0	0	5	(36.00, 108.00)[2]	(36.00, 108.00)[2](63.43, 116.57)[1](93.03, 161.30)[7]
	0	2	2	2	−3	2			(108.00, 36.00)[2](116.57, 63.43)[1](129.66, 149.52)[12]
	0	2	2	2	2	−3			(149.52, 129.66)[13](161.30, 93.03)[8](180.00, 180.00)[2]
	0	−3	2	2	2	2			(180.00, 180.00)[5]
	0	2	−3	2	2	2			
	0	2	2	−3	2	2			
9	1	0	2	0	2	0	3	(41.81, 138.19)[1]	(41.81, 138.19)[1](60.00, 60.00)[3](81.82, 167.34)[13]
	0	2	0	1	0	2			(99.59, 99.59)[11](109.47, 109.47)[4](124.31, 159.45)[22]
	2	0	1	0	−2	0			(138.19, 41.81)[1](146.44, 146.44)[27](159.45, 124.31)[21]
	0	1	0	2	0	−2			(167.34, 81.82)[12](180.00, 180.00)[3](180.00, 180.00)[6]
	0	−2	0	2	0	1			
	2	0	−2	0	1	0			
11	11	0	0	0	0	0	11	(19.46, 171.23)[2]	(19.46, 171.23)[2](52.54, 44.77)[2](65.34, 126.81)[8]
	0	2	6	−4	−1	8			(82.31, 132.79)[4](91.46, 27.23)[2](104.95, 165.78)[21]
	0	8	2	6	−4	−1			(117.30, 87.16)[13](124.54, 99.23)[2](124.54, 99.23)[5]
	0	−1	8	2	6	−4			(135.77, 156.90)[36](135.77, 156.90)[39](153.09, 142.19)[41]
	0	−4	−1	8	2	6			(163.46, 116.77)[2](163.46, 116.77)[32](169.80, 63.98)[11]
	0	6	−4	−1	8	2			(180.00, 180.00)[10]
11*	11	0	0	0	0	0	11	(27.23, 91.46)[2]	(27.23, 91.46)[2](44.77, 52.54)[2](63.98, 169.80)[11]
	0	6	−1	2	−4	8			(87.16, 117.30)[12](99.23, 124.54)[2](99.23, 124.54)[5]
	0	8	6	−1	2	−4			(116.77, 163.46)[2](116.77, 163.46)[32](126.81, 65.34)[7]
	0	−4	8	6	−1	2			(132.79, 82.31)[4](142.19, 153.09)[40](156.90, 135.77)[37]
	0	2	−4	8	6	−1			(156.90, 135.77)[38](165.78, 104.95)[22](171.23, 19.46)[2]
	0	−1	2	−4	8	6			(180.00, 180.00)[9]
16	2	−1	3	0	1	1	4	(1.04, 88.96)[3]	(31.04, 88.96)[3](50.49, 139.58)[7](72.00, 144.00)[5]
	3	2	−1	−1	−1	0			(82.82, 82.82)[11](88.96, 31.04)[3](98.24, 169.04)[37]
	−1	3	2	1	0	−1			(98.24, 169.04)[38](112.02, 112.02)[27](120.00, 120.00)[6]
	1	−1	0	3	−2	−1			(132.28, 162.22)[55](139.58, 50.49)[8](144.00, 72.00)[5]
	1	0	−1	1	3	−2			(151.04, 151.04)[3] (151.04, 151.04)[56](151.04, 151.04)[57]
	0	1	−1	2	1	3			(162.22, 132.28)[54](169.04, 98.24)[36](169.04, 98.24)[39]
									(180.00, 180.00)[14]
19	2	3	14	4	10	6	19	(20.72, 146.10)[3]	(20.72, 146.10)[3](56.75, 149.77)[4]
	14	2	3	−10	−6	4			(70.70, 101.48)[12](78.21, 71.22)[8](89.24, 170.76)[41]
	3	14	2	6	−4	−10			(99.28, 26.10)[3](105.12, 123.71)[40](114.12, 130.09)[9]
	6	−10	4	12	−8	−1			(127.80, 165.02)[60](127.80, 165.02)[61](135.86, 80.50)[21]
	10	−4	−6	1	12	−8			(140.72, 93.90)[3] (140.72, 93.90)[6](148.45, 155.64)[67]
	4	6	−10	8	1	12			(160.65, 140.09)[62](160.65, 140.09)[63] (168.08, 112.95)[55]
									(172.64, 53.34)[13](180.00, 180.00)[16]
19*	8	12	−1	10	6	−4	19	(26.10, 99.28)[3]	(26.10, 99.28)[3](53.34, 172.64)[12]
	−1	8	12	−6	4	10			(71.22, 78.21)[7](80.50, 135.86)[22](93.90, 140.72)[3]
	12	−1	8	−4	−10	−6			(93.90, 140.72)[6](101.48, 70.70)[13](112.95, 168.08)[54]
	−4	−6	10	14	−3	2			(123.71, 105.12)[41](130.09, 114.12)[10](140.09, 160.65)[64]
	6	−10	4	−2	14	−3			(140.9, 160.65)[65](146.10, 20.72)[3](149.77, 56.75)[4]
	10	−4	−6	3	−2	14			(155.64, 148.45)[66](165.02, 127.80)[58](165.02, 127.80)[59]
									(170.76, 89.24)[40](180.00, 180.00)[15]
20	3	2	7	−2	5	3	10	(26.57, 153.43)[1]	(26.57, 153.43)[1](51.09, 112.22)[8](61.73, 88.49)[7]
	−2	7	2	3	−5	3			(76.12, 171.86)[27](88.49, 61.73)[8](95.48, 130.88)[36]
	7	−2	3	2	−5	−3			(95.48, 130.88)[39](106.05, 136.35)[10](112.22, 51.09)[7]
	2	3	−2	7	5	−3			(121.76, 166.81)[58](121.76, 166.81)[59](130.88, 95.48)[37]
	3	−3	−3	3	0	8			(130.88, 95.48)[38](136.35, 106.05)[9](144.99, 158.58)[70]
	5	5	−5	−5	0	0			(144.99, 158.58)[71] (153.43, 26.57)[1](158.58, 144.99)[68]
									(158.58, 144.99)[69](166.81, 121.76)[60] (166.81, 121.76)[61]
									(171.86, 76.12)[27](180.00, 180.00)[17](180.00, 180.00)[18]

Table 1. *(cont.)*

Σ	$\mathbf{R}\times F$						F	Disorientation	Equivalent UST rotations
25	0	2	2	3	2	2	5	(37.40, 173.95)[8]	(37.40, 173.95)[8](53.13, 53.13)[1](60.96, 100.69)[13]
	3	2	−2	0	−2	2			(72.00, 144.00)[32](87.29, 147.91)[9](95.74, 95.74)[27]
	2	0	4	−2	−1	0			(100.69, 60.96)[12](108.34, 170.20)[62](108.34, 170.20)[63]
	2	1	0	2	0	−4			(120.00, 120.00)[56](120.00, 120.00)[57](126.87, 126.87)[1]
	2	−4	0	2	0	1			(126.87, 126.87)[14](137.58, 164.11)[73](144.00, 72.00)[32]
	2	0	−1	−2	4	0			(147.91, 87.29)[10] (154.16, 154.16)[74](154.16, 154.16)[75]
									(164.11, 137.58)[72] (170.20, 108.34)[64](170.20, 108.34)[65]
									(173.95, 37.40)[7] (180.00, 180.00)[19](180.00, 180.00)[20]
29	20	10	9	−10	12	−4	29	(34.34, 77.95)[1]	(34.34, 77.95)[1](45.98, 112.62)[11] (60.42, 148.84)[21]
	−10	24	10	5	−6	2			(78.76, 152.20)[10](88.46, 108.67)[40] (94.04, 82.98)[22]
	9	−10	20	10	−12	4			(102.59, 171.49)[68](102.59, 171.49)[69] (110.65, 52.32)[12]
	10	5	−10	24	6	−2			(115.43, 128.48)[67](122.93, 134.25)[16] (127.43, 38.72)[8]
	−4	−2	4	2	15	24			(134.53, 166.20)[77](141.45, 90.63)[54] (145.66, 102.05)[1]
	12	6	−12	−6	−16	15			(145.66, 102.05)[14](152.36, 157.59)[84] (152.36, 157.59)[85]
									(163.02, 143.34)[80](163.02, 143.34)[83] (169.53, 118.83)[73]
									(173.54, 69.16)[41] (180.00, 180.00)[23] (180.00, 180.00)[24]
29*	16	−6	12	12	−6	15	29	(38.72, 127.43)[7]	(38.72, 127.43)[7](52.32, 110.65)[13] (69.16, 173.54)[40]
	12	10	9	−20	10	4			(77.95, 34.34)[1](82.98, 94.04)[21] (90.63, 141.45)[55]
	−6	24	10	10	−5	−2			(102.05, 145.66)[1](102.05, 145.66)[14] (108.67, 88.46)[41]
	15	−2	4	4	−2	−24			(112.62, 45.98)[11](118.83, 169.53)[72] (128.48, 115.43)[66]
	−6	−5	10	10	24	−2			(134.25, 122.93)[15](143.34, 163.02)[81] (143.34, 163.02)[82]
	12	10	−20	9	10	4			(148.84, 60.42)[22](152.20, 78.76)[9] (157.59, 152.36)[86]
									(157.59, 152.36)[87](166.20, 134.53)[76] (171.49, 102.59)[70]
									(171.49, 102.59)[71](180.00, 180.00)[25] (180.00, 180.00)[26]
31_1	31	0	0	0	0	0	31	(13.29, 120.36)[2]	(13.29, 120.36)[2](58.71, 23.64)[2]
	0	12	6	3	−14	24			(78.72, 116.98)[39](85.29, 95.64)[2](109.62, 134.14)[71]
	0	24	12	6	3	−14			(117.95, 139.21)[17](122.91, 64.50)[21](130.71, 167.64)[2]
	0	−14	24	12	6	3			(130.71, 167.64)[79](138.27, 101.85)[63](150.13, 159.93)[93]
	0	3	−14	24	12	6			(157.29, 48.36)[2](168.70, 125.73)[77](173.02, 84.87)[56]
	0	6	3	−14	24	12			(180.00, 180.00)[29]
31_1^*	31	0	0	0	0	0	31	(23.64, 58.71)[2]	(23.64, 58.71)[2](48.36, 157.29)[2](64.50, 122.91)[22]
	0	24	6	−14	12	3			(84.87, 173.02)[57](95.64, 85.29)[2](101.85, 138.27)[64]
	0	3	24	6	−14	12			(116.98, 78.72)[37](120.36, 13.29)[2](125.73, 168.70)[76]
	0	12	3	24	6	−14			(134.14, 109.62)[68](139.21, 117.95)[17](155.13, 66.98)[6]
	0	−14	12	3	24	6			(159.93, 150.13)[95](167.64, 130.71)[2](167.64, 130.71)[78]
	0	6	−14	12	3	24			(180.00, 180.00)[28]
31_2	24	11	−4	12	2	−10	31	(35.13, 53.02)[3]	(35.13, 53.02)[3](48.36, 157.29)[5](72.86, 104.26)[21]
	−4	24	11	−2	10	12			(84.87, 173.02)[3](84.87, 173.02)[56](95.64, 85.29)[32]
	11	−4	24	−10	−12	−2			(101.85, 138.27)[65](111.36, 142.85)[15](116.98, 78.72)[38]
	−10	−2	12	26	−6	−1			(134.14, 109.62)[69](139.21, 117.95)[18](147.25, 161.67)[89]
	2	−12	10	1	26	−6			(147.25, 161.67)[91](152.14, 42.36)[12](155.13, 66.98)[3]
	12	−10	−2	6	1	26			(159.93, 150.13)[94](167.64, 130.71)[79](172.37, 95.13)[67]
									(180.00, 180.00)[30]
31_2^*	4	10	11	12	−2	24	31	(42.36, 152.14)[13]	(42.36, 152.14)[13](53.02, 35.13)[3](66.98, 155.13)[3]
	−2	26	10	−6	1	−12			(78.72, 116.98)[36](85.29, 95.64)[32](95.13, 172.37)[66]
	24	−2	4	10	−12	−11			(104.26, 72.86)[22](109.62, 134.14)[70](117.95, 139.21)[18]
	10	−6	12	−1	26	−2			(130.71, 167.64)[78](138.27, 101.85)[62](142.85, 111.36)[16]
	11	12	−24	2	10	4			(150.13, 159.93)[92](157.29, 48.36)[5](161.67, 147.25)[88]
	12	−1	2	−26	−6	10			(161.67, 147.25)[90](173.02, 84.87)[3](173.02, 84.87)[57]
									(180.00, 180.00)[31]
36_1	1	4	1	3	3	0	6	(15.52, 135.52)[3]	(15.52, 135.52)[3](60.31, 174.48)[39](70.53, 70.53)[4]
	1	1	4	−3	0	3			(76.24, 108.73)[38](84.79, 147.23)[60](104.48, 104.48)[3]
	4	1	1	0	−3	−3			(108.73, 76.24)[36](115.39, 171.06)[83](125.69, 125.69)[75]
	0	−3	3	4	−1	1			(131.81, 131.81)[19](131.81, 131.81)[20](135.52, 15.52)[3]
	3	−3	0	−1	4	−1			(141.43, 165.51)[98](147.23, 84.79)[58](156.44, 156.44)[102]
	3	0	−3	1	−1	4			(165.51, 141.43)[101](171.06, 115.39)[81](174.48, 60.31)[37]
									(180.00, 180.00)[33]

Table 1. *(cont.)*

Σ	$\mathbf{R}\times F$						F	Disorientation	Equivalent UST rotations
36_2	4	1	−1	4	−1	1	6	(39.00, 121.82)[11]	(39.00, 121.82)[11](48.19, 48.19)[1](60.31, 174.48)[36]
	4	1	1	−4	1	1			(76.24, 108.73)[37](84.79, 147.23)[61](97.31, 150.77)[16]
	−1	2	5	1	−1	2			(104.48, 104.48)[56](104.48, 104.48)[57](108.73, 76.24)[39]
	1	1	2	1	2	−5			(115.39, 171.06)[80](121.82, 39.00)[11](125.69, 125.69)[74]
	1	−5	2	1	2	1			(131.81, 131.81)[1](141.43, 165.51)[96](141.43, 165.51)[99]
	−1	2	−1	1	5	2			(147.23, 84.79)[59](150.77, 97.31)[15](156.44, 156.44)[103]
									(165.51, 141.43)[97](165.51, 141.43)[100](171.06, 115.39)[82]
									(174.48, 60.31)[38](180.00, 180.00)[34](180.00, 180.00)[35]
41_1	41	0	0	0	0	0	41	(11.11, 128.87)[2]	(11.11, 128.87)[2](60.89, 87.13)[2](67.67, 117.73)[41]
	0	14	26	−22	6	17			(77.52, 151.00)[58](83.11, 15.13)[2](111.30, 172.06)[88]
	0	17	14	26	−22	6			(118.22, 66.44)[36](122.38, 132.21)[84](128.93, 137.52)[23]
	0	6	17	14	26	−22			(132.89, 56.87)[2](139.18, 167.14)[105](149.10, 108.22)[20]
	0	−22	6	17	14	26			(155.11, 159.13)[2](170.56, 123.38)[96](174.17, 79.76)[66]
	0	26	−22	6	17	14			(180.00, 180.00)[43]
41_1^*	41	0	0	0	0	0	41	(15.13, 83.11)[2]	(15.13, 83.11)[2](56.87, 132.89)[2](66.44, 118.22)[38]
	0	26	17	−22	14	6			(79.76, 174.17)[67](87.13, 60.89)[2](108.22, 149.10)[19]
	0	6	26	17	−22	14			(117.73, 67.67)[40](123.38, 170.56)[97](128.87, 11.11)[2]
	0	14	6	26	17	−22			(132.21, 122.38)[86](137.52, 128.93)[26](151.00, 77.52)[60]
	0	−22	14	6	26	17			(159.13, 155.11)[2](167.14, 139.18)[106](172.06, 111.30)[89]
	0	17	−22	14	6	26			(180.00, 180.00)[42]
41_2	30	−4	11	4	−12	22	41	(30.90, 71.78)[1]	(30.90, 71.78)[1](48.16, 175.10)[22](60.89, 87.13)[5]
	4	35	−4	6	−18	−8			(77.52, 151.00)[59](91.55, 154.12)[17](91.55, 154.12)[18]
	11	4	30	−4	12	−22			(99.43, 114.16)[67](104.08, 91.44)[55](111.30, 172.06)[90]
	−4	6	4	35	18	8			(118.22, 66.44)[39](122.38, 132.21)[85](128.93, 137.52)[24]
	22	8	−22	−8	24	−3			(132.89, 56.87)[32](139.18, 167.14)[104](145.34, 98.10)[72]
	−12	18	12	−18	13	24			(149.10, 108.22)[1](149.10, 108.22)[19](155.11, 159.13)[117]
									(161.05, 36.92)[4](164.69, 145.91)[108](170.56, 123.38)[98]
									(170.56, 123.38)[99](180.00, 180.00)[8](180.00, 180.00)[44]
41_2^*	3	8	22	22	8	24	41	(36.92, 161.05)[4]	(36.92, 161.05)[4](56.87, 132.89)[32](66.44, 118.22)[37]
	22	4	11	−30	4	12			(71.78, 30.90)[1](87.13, 60.89)[5](91.44, 104.08)[54]
	8	35	4	4	−6	−18			(98.10, 145.34)[73](108.22, 149.10)[1](108.22, 149.10)[20]
	24	−18	12	12	−18	−13			(114.16, 99.43)[66](123.38, 170.56)[100](123.38, 170.56)[101]
	8	−6	4	4	35	−18			(132.21, 122.38)[87](137.52, 128.93)[25](145.91, 164.69)[109]
	22	4	−30	11	4	12			(151.00, 77.52)[61](154.12, 91.55)[17](154.12, 91.55)[18]
									(159.13, 155.11)[116](167.14, 139.18)[107](172.06, 111.30)[91]
									(175.10, 48.16)[21](180.00, 180.00)[7](180.00, 180.00)[45]
44	10	3	2	11	−5	15	22	(27.95, 175.55)[7]	(27.95, 175.55)[7](47.21, 97.69)[4](56.01, 123.99)[27]
	2	5	18	−11	−1	3			(68.04, 153.72)[54](74.61, 51.61)[11](78.44, 44.88)[7]
	3	13	5	11	4	−12			(84.31, 156.53)[15](93.18, 120.85)[70](93.18, 120.85)[71]
	15	−12	3	0	9	−5			(98.34, 101.30)[60](98.34, 101.30)[61](106.30, 172.79)[94]
	−5	4	−1	0	19	9			(106.30, 172.79)[95](113.86, 81.11)[55](118.37, 136.83)[92]
	11	11	−11	−11	0	0			(118.37, 136.83)[93](125.46, 141.58)[29](125.46, 141.58)[31]
									(129.73, 74.00)[54](136.49, 168.33)[112](136.49, 168.33)[113]
									(136.49, 168.33)[114](143.09, 106.94)[80](143.09, 106.94)[83]
									(147.10, 115.66)[23](147.10, 115.66)[24](153.51, 161.06)[125]
									(153.51, 161.06)[126](157.43, 31.21)[11](159.84, 61.04)[10]
									(163.72, 149.12)[121](163.72, 149.12)[122](163.72, 149.12)[123]
									(169.96, 128.97)[104](169.96, 128.97)[105](173.80, 91.64)[74]
									(173.80, 91.64)[75](180.00, 180.00)[47]
44*	13	11	−5	12	4	−3	22	(31.21, 157.43)[11]	(31.21, 157.43)[11](44.88, 78.44)[8](51.61, 74.61)[11]
	12	0	3	−5	−9	15			(61.04, 159.84)[9](74.00, 129.73)[55](81.11, 113.86)[54]
	−5	11	18	3	1	2			(91.64, 173.80)[74](91.64, 173.80)[75](97.69, 47.21)[4]
	11	−11	11	0	0	−11			(101.30, 98.34)[58](101.30, 98.34)[59](106.94, 143.09)[81]
	−3	−11	2	15	5	10			(106.94, 143.09)[82](115.66, 147.10)[25](115.66, 147.10)[26]
	4	0	1	−9	19	5			(120.85, 93.18)[68](120.85, 93.18)[69](123.99, 56.01)[27]
									(128.97, 169.96)[106](128.97, 169.96)[107](136.83, 118.37)[94]
									(136.83, 118.37)[95](141.58, 125.46)[28](141.58, 125.46)[30]
									(149.12, 163.72)[118](149.12, 163.72)[119](149.12, 163.72)[120]
									(153.72, 68.04)[55](156.53, 84.31)[16](161.06, 153.51)[124]
									(161.06, 153.51)[127](168.33, 136.49)[110](168.33, 136.49)[111]
									(168.33, 136.49)[115](172.79, 106.30)[92](172.79, 106.30)[93]
									(175.55, 27.95)[8](180.00, 180.00)[46]

Table 1. *(cont.)*

Σ	$\mathbf{R}\times F$						F	Disorientation	Equivalent UST rotations
45	8	−2	7	2	−2	10	15	(21.62, 105.25)[1]	(21.62, 105.25)[1](54.64, 155.79)[38](63.00, 67.70)[12]
	2	12	−2	3	−8	0			(74.75, 158.38)[14](85.10, 125.83)[65](91.01, 108.41)[58]
	7	2	8	−2	2	−10			(99.98, 173.35)[86](108.41, 91.01)[61](113.39, 140.32)[91]
	−2	3	2	12	8	0			(121.17, 144.66)[28](125.83, 85.10)[63](128.66, 37.68)[13]
	10	0	−10	0	5	0			(133.18, 169.24)[111](133.18, 169.24)[115](140.32, 113.39)[88]
	−2	8	2	−8	8	5			(144.66, 121.17)[31](155.79, 54.64)[39](158.38, 74.75)[1]
									(162.54, 151.57)[128](162.54, 151.57)[129](169.24, 133.18)[113]
									(173.35, 99.98)[85](180.00, 180.00)[48](180.00, 180.00)[49]
45*	8	2	8	−5	8	2	15	(37.68, 128.66)[12]	(37.68, 128.66)[12](54.64, 155.79)[37](67.70, 63.00)[13]
	8	2	3	0	−12	2			(74.75, 158.38)[1](85.10, 125.83)[64](91.01, 108.41)[59]
	2	8	2	10	2	−7			(99.98, 173.35)[87](105.25, 21.62)[1](108.41, 91.01)[60]
	2	−7	2	10	2	8			(113.39, 140.32)[89](121.17, 144.66)[30](125.83, 85.10)[62]
	8	2	−12	0	3	2			(133.18, 169.24)[110](140.32, 113.39)[90](144.66, 121.17)[29]
	−5	10	0	0	0	10			(151.57, 162.54)[130](151.57, 162.54)[131](155.79, 54.64)[36]
									(158.38, 74.75)[14](169.24, 133.18)[112](169.24, 133.18)[114]
									(173.35, 99.98)[84](180.00, 180.00)[50](180.00, 180.00)[51]
49_1	2	0	5	0	2	4	7	(16.60, 163.40)[1]	(16.60, 163.40)[1](58.45, 126.49)[41](64.62, 64.62)[4]
	0	5	0	2	−4	2			(73.64, 174.89)[70](81.79, 81.79)[6](86.50, 114.72)[63]
	5	0	2	0	−2	−4			(104.60, 152.98)[23](110.92, 110.92)[75](114.72, 86.50)[64]
	0	2	0	5	4	−2			(120.69, 171.72)[108](126.49, 58.45)[40](130.01, 130.01)[102]
	4	−2	−4	2	0	3			(130.01, 130.01)[103](135.58, 135.58)[34](135.58, 135.58)[35]
	2	4	−2	−4	3	0			(144.39, 166.59)[133](152.98, 104.60)[26](158.21, 158.21)[63]
									(163.40, 16.60)[1](166.59, 144.39)[132](171.72, 120.69)[109]
									(174.89, 73.64)[69](180.00, 180.00)[11](180.00, 180.00)[52]
49_2	6	−2	3	0	0	0	7	(38.21, 38.21)[3]	(38.21, 38.21)[3](46.92, 138.98)[21](73.64, 174.89)[71]
	3	6	−2	0	0	0			(81.79, 81.79)[3](86.50, 114.72)[62](93.73, 149.72)[77]
	−2	3	6	0	0	0			(104.60, 152.98)[24](110.92, 110.92)[74](114.72, 86.50)[65]
	0	0	0	6	−3	−2			(135.58, 135.58)[33](138.98, 46.92)[22](144.39, 166.59)[135]
	0	0	0	2	6	−3			(149.72, 93.73)[76](152.98, 104.60)[25](158.21, 158.21)[3]
	0	0	0	3	2	6			(158.21, 158.21)[136](166.59, 144.39)[134](174.89, 73.64)[68]
									(180.00, 180.00)[53]

Q-ROTs lie along straight lines and planes (and at all the intersections of these straight lines and planes) in F–R space. A group of rotation tiles, lying within the unit stereographic triangle, with rotation angles up to 75°, is shown in Fig. 4. The planes and the lines represented in Fig. 4 are planes and lines passing through the three represented $\Sigma 1$ vertices and other $\Sigma 1$ vertices (not included in Fig. 4). $\Sigma 4$, $\Sigma 5$ and $\Sigma 9$ vertices can be found at the intersections of the above planes and lines. This suggests (although we do not possess a complete proof) that starting with the positions of $\Sigma 1$ vertices one can iteratively derive the positions of all other Q-ROTs in the F–R space. At each step of the iteration, new planes are drawn, passing through any three non-collinear available Q-ROT vertices. New vertices, arising as intersections of at least three such planes, are added to the set of Q-ROT vertices that are available at the next step. Let us also mention that all Q-ROTs with $\Sigma < 50$ can be found on the faces of the rotation tiles, as shown in Fig. 5.

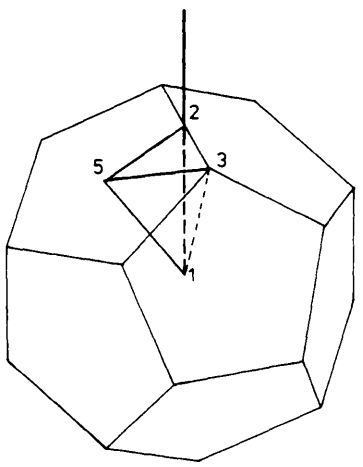

Fig. 3. Perspective of pentagonal dodecahedron showing a standard disorientation tile defined by Q-ROT with $\Sigma = 1, 4, 5, 9$.

A similar line structure exists for twin rotations (rotations through 180°) lying on the surface of the infinite radius sphere in the F–R space. To show this, let us represent rotations by vectors $\omega\mathbf{n}$, thus mapping 180° rotations onto the surface of a finite radius sphere, and form a gnomonic projection of this surface. Great circles are transformed to straight lines and each face of a rotation tile is represented as a triangle in this projection, which therefore contains every value of $\Sigma < 50$. A part of this triangle tiling is shown in Fig. 6. The only

Table 2. *Axis identification for Table 1*

The Σ value holds for the 180° rotation around the quoted axis. The density (number of vertex points/unit length) of the axis scales as $1/\Omega_2$. Positions of some of these axes are shown in Fig. 6.

No.	Indices	Ω_2^2	Σ	No.	Indices	Ω_2^2	Σ	No.	Indices	Ω_2^2	Σ
[1]	[0 1 0 1 0 0]	4	1	[47]	[3 1 0 1 −1 0]	176	44	[93]	[2 2 1 2 1 1]	449	449
[2]	[1 0 0 0 0 0]	5	5	[48]	[2 1 2 −1 1 −1]	180	45	[94]	[1 −3 0 −2 −1 0]	449	449
[3]	[0 0 0 1 −1 1]	9	9	[49]	[1 0 3 0 1 1]	180	45	[95]	[2 −2 2 −1 −1 1]	449	449
[4]	[1 0 0 1 −1 1]	16	4	[50]	[1 1 1 2 −1 2]	180	45	[96]	[2 0 2 1 −1 1]	449	505
[5]	[0 1 1 1 0 1]	20	5	[51]	[3 0 0 1 −1 1]	180	45	[97]	[0 1 1 2 −1 2]	449	505
[6]	[0 0 2 0 1 1]	36	9	[52]	[1 0 1 2 −2 2]	196	49	[98]	[3 1 0 1 0 0]	449	505
[7]	[0 1 1 0 1 0]	41	41	[53]	[0 3 0 2 1 0]	196	49	[99]	[1 2 1 2 0 1]	449	505
[8]	[1 1 0 1 0 0]	41	41	[54]	[1 0 2 −1 1 0]	209	209	[100]	[2 2 −1 1 0 −1]	449	505
[9]	[1 0 2 0 0 1]	44	11	[55]	[1 1 2 0 1 0]	209	209	[101]	[0 0 3 0 1 1]	449	505
[10]	[2 1 0 0 0 −1]	44	11	[56]	[2 −2 −1 −2 −1 −1]	225	225	[100]	[2 2 −1 1 0 −1]	449	505
[11]	[1 0 −2 0 −1 −1]	49	49	[57]	[3 −1 −1 0 −2 0]	225	225	[103]	[0 2 −3 0 1 −3]	529	529
[12]	[1 1 1 1 0 1]	61	61	[58]	[2 0 0 1 −1 1]	241	241	[104]	[2 2 1 0 1 −1]	569	569
[13]	[1 −1 1 0 −1 1]	61	61	[59]	[0 2 1 1 1 0]	241	241	[105]	[1 1 1 2 0 2]	569	569
[14]	[2 −1 1 0 −1 1]	64	16	[60]	[1 0 2 0 1 1]	241	241	[106]	[2 −1 2 0 −1 1]	569	569
[15]	[1 1 0 2 −1 1]	76	19	[61]	[2 1 0 1 −1 0]	241	241	[107]	[1 2 1 0 2 −1]	569	569
[16]	[2 0 1 1 −1 1]	76	19	[62]	[1 −1 −2 −1 −1 −1]	261	261	[108]	[3 −1 1 −1 −1 0]	589	589
[17]	[1 2 1 0 1 −1]	80	20	[63]	[1 1 1 −1 2 −1]	261	261	[109]	[3 1 1 1 −1 0]	589	589
[18]	[0 1 2 1 1 1]	80	20	[64]	[2 1 1 1 −1 1]	261	261	[110]	[3 1 0 0 0 −1]	601	601
[19]	[2 0 0 1 −2 1]	100	25	[65]	[1 1 2 1 1 1]	261	261	[111]	[0 2 1 2 1 1]	601	601
[20]	[1 2 −1 2 0 0]	100	25	[66]	[0 1 −3 1 −1 −1]	269	269	[112]	[2 1 0 2 −1 1]	601	601
[21]	[2 0 0 0 −1 0]	109	109	[67]	[3 1 1 1 0 1]	269	269	[113]	[3 0 1 0 −1 0]	601	601
[22]	[2 0 1 0 0 0]	109	109	[68]	[1 −1 −1 −2 0 −2]	281	281	[114]	[0 2 2 1 1 1]	601	601
[23]	[2 0 2 0 −1 1]	116	29	[69]	[2 1 0 −1 1 −2]	281	281	[115]	[1 0 2 1 −1 2]	601	601
[24]	[3 0 1 0 0 0]	116	29	[70]	[2 2 1 1 1 0]	281	281	[116]	[1 −1 −3 1 −3 0]	605	605
[25]	[3 0 0 0 −1 0]	116	29	[71]	[1 2 2 1 0 1]	281	281	[117]	[3 1 3 1 0 1]	605	605
[26]	[0 1 1 2 0 2]	116	29	[72]	[0 0 2 1 0 2]	341	341	[118]	[2 1 3 0 0 1]	641	641
[27]	[1 2 −1 0 1 −2]	121	121	[73]	[2 0 2 0 0 1]	341	341	[119]	[2 1 2 2 −1 1]	641	641
[28]	[0 2 1 2 0 1]	124	31	[74]	[0 1 −1 −2 2 −3]	361	361	[120]	[3 1 2 0 1 0]	641	641
[29]	[2 2 0 1 0 −1]	124	31	[75]	[3 1 −2 0 −1 −2]	361	361	[121]	[3 0 −1 1 −2 0]	641	641
[30]	[2 0 2 −1 1 0]	124	31	[76]	[2 1 1 −1 1 −1]	389	389	[122]	[1 2 1 −1 2 −2]	641	641
[31]	[1 0 2 1 0 2]	124	31	[77]	[1 1 1 2 −1 1]	389	389	[123]	[0 3 0 1 2 −1]	641	641
[32]	[1 0 1 1 −1 1]	125	125	[78]	[1 2 0 2 0 0]	405	405	[124]	[1 −2 3 −1 0 2]	649	649
[33]	[1 1 2 −1 2 −1]	144	36	[79]	[2 0 2 −1 0 0]	405	405	[125]	[3 2 1 2 0 1]	649	649
[34]	[3 −1 1 −1 0 0]	144	36	[80]	[3 0 0 −1 0 −1]	409	409	[126]	[2 2 3 1 1 0]	649	649
[35]	[1 −2 −2 −1 −1 −1]	144	36	[81]	[1 2 2 1 1 0]	409	409	[127]	[1 0 −2 −2 1 −3]	649	649
[36]	[1 2 1 1 0 0]	145	145	[82]	[3 1 1 0 0 0]	409	409	[128]	[1 3 −1 1 1 −2]	661	661
[37]	[0 1 0 2 −1 1]	145	145	[83]	[1 2 −1 2 −1 0]	409	409	[129]	[3 1 −2 1 −1 −1]	661	661
[38]	[2 −1 1 −1 0 0]	145	145	[84]	[3 2 2 0 0 0]	421	421	[130]	[3 1 2 1 −1 1]	661	661
[39]	[2 1 1 0 1 0]	145	145	[85]	[2 2 2 2 0 1]	421	421	[131]	[2 1 3 1 1 1]	661	661
[40]	[2 1 2 0 0 0]	149	149	[86]	[0 3 0 0 2 −2]	421	421	[132]	[2 2 0 0 1 −2]	701	701
[41]	[0 2 −1 2 0 0]	149	149	[87]	[2 1 −2 2 −2 0]	421	421	[133]	[2 0 2 1 0 2]	701	701
[42]	[3 0 1 −1 0 −1]	164	41	[88]	[1 −2 −2 0 −2 0]	445	445	[134]	[0 3 0 2 0 0]	701	701
[43]	[3 1 1 0 0 −1]	164	41	[89]	[2 2 1 2 0 0]	445	445	[135]	[3 0 2 0 0 0]	701	701
[44]	[1 2 1 2 −1 1]	164	41	[90]	[1 0 0 2 −2 2]	445	445	[136]	[2 −2 3 −3 1 0]	729	729
[45]	[2 1 1 −1 2 −1]	164	41	[91]	[2 2 2 0 1 0]	445	445				
[46]	[0 1 3 0 1 1]	176	44	[92]	[3 2 1 1 0 0]	449	449				

points of the F–R space not represented belong to the interiors of the rotation tiles, therefore any disorientation not having a twin representation* lies within the rotation tile and has a value of $\Sigma > 50$.

6.1. *Multiplicity N_Σ of equivalent rotations*

Although the rotation tiles vary in shape and size, according to their relative orientation and displacement with respect to the standard disorientation tile, the great advantage of the F–R space is that it is easy to visualize the packing of the tetrahedra and to build a corresponding 3D model.

When the point representing a vector in the F–R space within or on the boundary of the rotation tile is known, it is easy to determine visually the multiplicity number N_Σ of distinct rotations that are either equivalent or inversely equivalent (therefore represent the same disorientation of the two grains) to a given disorientation and the numbers are presented in Table 3. This follows from the connectivity of the tiles. First, the number N_T

* We say that a disorientation has a twin representation if it can be obtained by a mirror reflection in a twin plane, or equivalently by a 180° rotation about a twin axis orthogonal to the twin plane (we do not discuss here the complications of non-centrosymmetric structures).

of tiles is found sharing a common Σ vertex in the rotation space. Fig. 4 clearly shows that for example a rotation corresponding to $\Sigma = 5$ is shared between 20 neighbouring tiles. There are 60 rotation tiles within the solid angle of one unit (standard) stereographic triangle and 120 such triangles in the 4π solid angle, whence $N_\Sigma = 120 \times 60/N_T$.

The computation of the multiplicity N_Σ^{UST} of all equivalent F–R vectors inside or on the boundary of the unit stereographic triangle (UST) is more involved but similar (Table 3). Any rotation, equivalent to a given disorientation, is conjugate to one of the above N_Σ^{UST} rotations. For this reason, we decided to include in column 5 of Table 1 only these N_Σ^{UST} rotations and not the complete set of N_Σ symmetry-related rotations.

Table 3. *Dependence of the multiplicities N_Σ and N_Σ^{UST} on the position in the standard disorientation tile*

Position in tile	N_T	$N_\Sigma/60$	N_Σ^{UST}	Σ values
Vertex $\Sigma 1$	120	1	8	1
$\Sigma 4$	24	5	8	4
$\Sigma 5$	20	6	10	5
$\Sigma 9$	12	10	12	9
Edge $\Sigma 1$–$\Sigma 5$	10	12	16	11, 11*, 31_1, 31_1^*, 41_1, 41_1^*
$\Sigma 1$–$\Sigma 4$, $\Sigma 4$–$\Sigma 9$	6	20	19	16, 19, 19*, 31_2, 31_2^*, 36_1, 49_2
$\Sigma 1$–$\Sigma 9$, $\Sigma 4$–$\Sigma 5$, $\Sigma 5$–$\Sigma 9$	4	30	24	20, 25, 29, 29*, 36_2, 41_2, 41_2^*, 45, 45*, 49_1
Any face	2	60	38	44, 44*

Table 4. *Proportion of random rotations close to Σ rotations according to the $\Sigma^{-1/2}$ criterion*

Cubic			Icosahedral		
Σ	N_Σ	Proportion $\times 10^{-2}$	Σ	N_Σ	Proportion $\times 10^{-2}$
1	24	1.98	1	60	4.95
3	96	1.53	4	300	3.10
5	144	1.07	5	360	2.68
7	192	0.86	9	600	1.83
9	288	0.88	11	720	1.70
11	288	0.668	11*	720	1.70
Total 6.98×10^{-2}			Total 15.96×10^{-2}		

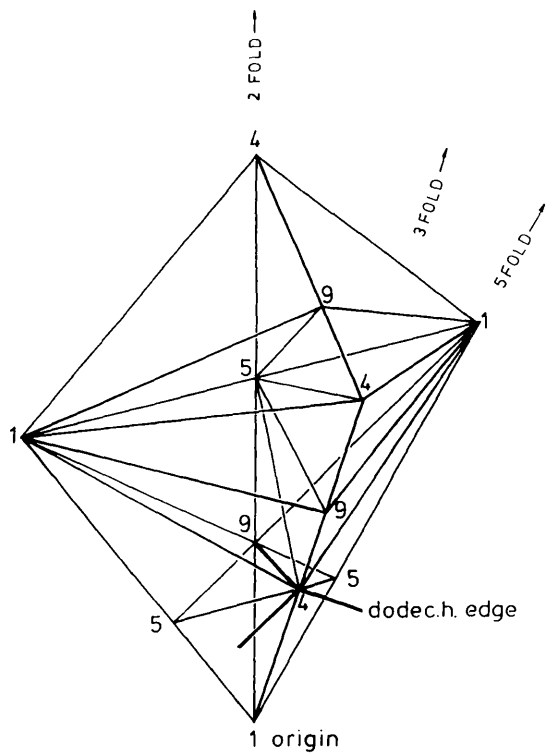

Fig. 4. Perspective of rotation tiles showing connectivity and sequence of vertices Σ = 1, 4, 5, 9.

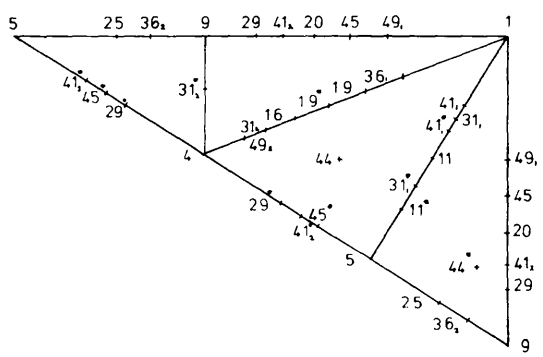

Fig. 5. Surface of standard disorientation tile opened out and plotted as its equivalent surface at 180° with positions of Q-ROT for $\Sigma < 50$.

6.2. *CSL order in a boundary of random rotation*

The presence of CSL order or DSC Burgers vectors in a grain boundary will affect the ease of diffusion, boundary migration and nucleation of second phases

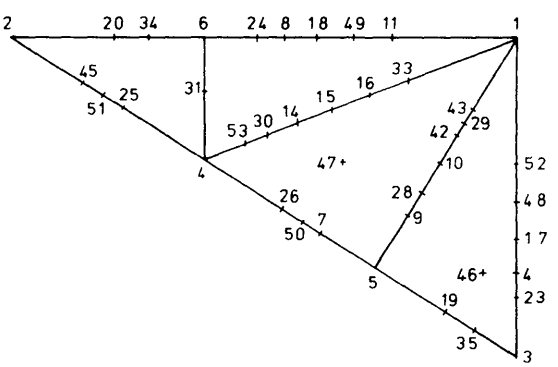

Fig. 6. Gnomonic projection of the 180° sphere (containing all 180° rotations) showing the positions of those axes from Table 2 generating twins with $\Sigma < 50$. Lines and triangles are equivalent to edges and faces of the standard disorientation tile, respectively. Certain Σ values are common for two non-equivalent axes (two non-equivalent points on the sphere) that provide two twin descriptions (*e.g.* $\Sigma 5$, $\Sigma 9$ but not $\Sigma 4$).

Table 5. *DSC and CSL bases for a few important cases in a reduced form, that is of basis vectors chosen to be of minimum length in 6D, together with corresponding disorientation angle*

Rotation	CSL basis vectors	DSC basis vectors	Rotation	CSL basis vectors	DSC basis vectors
36° [2] Σ	1 0 0 0 0 0	5 0 0 0 0 0	44.48° [3] Σ4	1 0 0 0 0 0	1 1 1 $\frac{1}{4}$ 1 $\bar{1}$
	0 1 $\bar{1}$ 0 0 0	0 1 $\bar{4}$ 1 1 1		1 0 1 $\bar{1}$ 0 0	0 0 1 $\bar{1}$ 0 0
	0 1 $\bar{1}$ 1 0 0	$\frac{1}{2}$ 0 1 1 $\bar{4}$ 1 1		1 0 0 0 1 $\bar{1}$	$\frac{1}{2}$ $\bar{1}$ 1 0 0 $\bar{1}$ 1
	0 1 0 0 $\bar{1}$ 1	0 1 1 1 $\bar{4}$ 1		0 1 0 0 1 1	$\bar{1}$ 1 0 0 1 1
	0 1 0 0 $\bar{1}$ 1	0 1 1 1 1 $\bar{4}$		0 $\bar{1}$ 1 1 0 0	0 0 1 1 0 0
	0 1 0 0 0 $\bar{1}$	0 1 1 1 1 1		0 1 0 0 0 0	1 $\bar{1}$ 1 1 1 1
19.46° [2] Σ11	1 0 0 0 0 0	11 0 0 0 0 0 0	41.81° [1] Σ9	1 0 0 0 1 1	$\bar{1}$ 0 2 1 0 0
	0 1 1 0 0 $\bar{1}$	0 5 4 1 3 $\bar{2}$		0 1 1 $\bar{1}$ 0 0	0 $\bar{1}$ 0 0 2 1
	0 1 1 1 0 0	$\frac{1}{11}$ 0 $\bar{2}$ 5 4 1 3		1 0 0 0 $\bar{1}$ 0	$\frac{1}{3}$ 1 0 1 2 0 0
	0 1 $\bar{1}$ 1 1 0	0 3 $\bar{2}$ 5 4 1		0 1 0 1 0 0	0 1 0 0 1 2
	0 1 0 $\bar{1}$ 1 1	0 1 3 $\bar{2}$ 5 4		0 0 1 1 0 0	0 1 0 0 1 $\bar{1}$
	0 1 0 0 $\bar{1}$ 1	0 4 1 3 $\bar{2}$ 5		0 0 0 0 $\bar{1}$ 1	1 0 1 $\bar{1}$ 0 0

and will lower the energy of the boundary from that of a random structure. Given a set of boundaries of rotation axis and angle chosen with random probability, what proportion will retain order characteristic of a CSL rotation? This calculation for cubic boundaries (Warrington & Boon, 1975) was based on the assumption that the rotation would need to lie within an angular deviation v proportional to $\Sigma^{-1/2}$ and that the number within a deviation v from a given rotation varies as $N_\Sigma(v - \sin v)/\pi \simeq N_\Sigma v^3/6\pi$ for small v. Table 4 compares the proportions expected for cubic and icosahedral boundaries and it is seen that for the lower Σ values the higher symmetry of the icosahedral phase approximately doubles the proportion of boundaries on the assumption that similar criteria apply. The presence of any texture that destroys a random distribution of rotations may be expected to increase the above proportions significantly.

7. CSL geometry, dense planes of coincident vertices

The 6D CSL can be derived from the 6D **R** matrix *via* the *O*-lattice theory (Bollmann, 1970) or by defining a basis matrix with determinant equal to Σ (see Warrington, 1993; Warrington & Lück, 1995). The basis matrix is traditionally expressed in reduced form with six column vectors being as nearly orthogonal as possible consistent with being of minimum length. The reduced bases for several low-order Σs are given in Table 5.

The coincident vertices are often not uniformly distributed over the 6D CSL but frequently occur as widely spaced planes with a dense packing of points within them. We conjecture that when there is a twin plane then this is the densest plane in the CSL.* All the vertices in the physical twin plane project from a 4D sublattice L_4 of the hyperlattice and one defines the vertex density ρ_4 of the latter as the inverse of the volume Ω_4 of its unit cell:

$$\rho_4 = 1/\Omega_4. \tag{14}$$

The physical twin axis, orthogonal to the physical twin plane, contains vertices that project from a 2D sublattice L_2 of unit-cell surface Ω_2 (see Table 2). The subspaces that embed L_4 and L_2 are orthogonal and, for a primitive hypercubic lattice of lattice constant a,

$$\Omega_4 = a^2\Omega_2. \tag{15}$$

The vertex density of L_2 is

$$\rho_2 = 1/\Omega_2. \tag{16}$$

For twin representable disorientations and odd twin axes (odd sum of indices, see Appendix *A*), a basis of the CSL can be obtained by adding to the basis vectors of L_4 the basis vectors of L_2, therefore CSL $= L_2 \oplus L_4$. Centrings are necessary if the twin axis is even (even sum of indices). Therefore, the CSL preserves complete 4D sublattices of the 6D hyperlattice in the family parallel to L_4. Σ is then the 'preservation index', one in Σ of such 4D sublattices of the hyperlattice belongs to the CSL. When the CSL has no twin description, the preserved 4D sublattices must be replaced with 2D sublattices (parallel to the sublattice L_2, corresponding to the rotation axis).

All this is valid also for CSL in a 3D lattice $\mathcal{L}$. The presence of a twin plane implies that the CSL is made of complete 2D lattice planes of $\mathcal{L}$, parallel to the twin plane. In general, the CSL is composed of complete 1D rows of $\mathcal{L}$, parallel to the rotation axis. For twin representable disorientations, both descriptions (in terms of preserved lattice planes and rows) are valid.

Because CSL lattices are special types of derivative lattice, this may be connected to Harker's classification (Harker, 1978; Rolley-Le Coz, Senechal & Billiet, 1983) of derivative lattices. CSLs with twin planes correspond

* In certain cases there are two twin planes, but the one orthogonal to an even twin axis is always more dense [see Radulescu (1994, 1995) and Appendix *A*].

to the third case of this classification, when complete planes of the basic lattice are preserved in the derivative lattice and CSLs with no twin planes correspond to the second case when only rows and no complete planes are preserved. There are always sublattices of the hyperlattice that are entirely included in the CSL, so that derivative lattices of the first kind in Harker's classification cannot be a CSL.

The above geometry of the CSL is reproduced in the CQL. The coincidence quasilattice frequently shows families of parallel planes of high density of coincident vertices. The planar density of coincidences (number of coincident vertices/unit surface) in the planes of such a family varies from zero to a maximum value (proportional to ρ_4 if the planes of the family are parallel to the twin plane). For some very dense twin planes, there are thin bands of coincidences, which are parallel to the twin plane and are separated by large intervals containing no coincidence. This is the case of $\Sigma 5$ and $\Sigma 9$ [for which Ω_2 and consequently Ω_4 are small, see (14), (15), (16)], as can be seen from the distribution of coincidence points in the Wieringa roofs in Figs. 2(*c*) and (*d*). For $\Sigma 4$, the coincident vertices are more homogeneously distributed in space, with no empty large intervals between vertex planes as seen in Fig. 2(*b*). The twofold axis has been chosen for Fig. 2 since it displays the homogeneity or the non-homogeneity more clearly than other roof orientations.

8. The DSC lattice, atomic rearrangements and grain boundary displacements

The DSC lattice is defined as the set of all the shift vectors that maintain the CSL (with displaced origin) and for simple hypercubic lattices is conveniently derived (Grimmer, Bollmannn & Warrington, 1974) *via* the equation

$$\mathbf{CSL}^T\,\mathbf{DSC} = 1, \qquad (17)$$

where $\mathbf{CSL}^T$ is the transpose of the matrix of basis column vectors for the CSL and **DSC** is the matrix of basis column DSC vectors.

Again, the reduced form of a basis for the DSC of several low-order Σs is given in Table 5. The corresponding shifts in physical space can be derived using (10) or the upper 3×6 part of the matrix **A** (equation 8).

The effect of a displacement of one icosahedral quasicrystal with respect to a second can be displayed by performing sideways shifts on well chosen Wieringa roofs. Provided the displacement corresponds to a vector in the 6D DSC lattice, the density of coincidences will remain the same in 6D. The density of coincidences in Wieringa roofs may decrease since these roofs have no periodic repeat. A fall in the density of coincidences may be restored in two ways. The first arises because the roof omits points in its neighbourhood as a result of its corrugation. The points may be revealed by a 'roof switching', *i.e.* replacing the concave (convex) assemblage of three lozenge faces having a common vertex with the convex (concave) assemblage opposite to it on the same rhombohedron and thus making the roof pass through another vertex of the 3D tiling. The second arises through a 'vertex flip', which moves a vertex to a new position not within the original tiling. This is referred to in the literature as a Bilinski or phason 'flip' (see Coxeter, 1973; Lück, 1988). The number of vertex flips necessary to restore coincidences can be estimated by using the perpendicular space. This number grows with the difference in size between the domains $\mathcal{A}$ and $\mathcal{D}$ (see §4) and therefore with the perpendicular component of the DSC shift (Radulescu & Warrington, 1995).

While 'switching' does not change the tiling, 'flipping' brings in new positions of vertices and produces loops of a special kind of linear topological defects [phasons (Lück, 1988)]. In a Wieringa roof chosen as close as possible to the interface such that it tests the coincidences in a neighbourhood of the interface, roof switching is the elementary deformation that leads to steps in the interface in order to look for high-density planes of the CQL. Thus, displacement of one quasicrystal with respect to the other by a DSC vector will generally shift the dense rows of coincident vertices in Figs. 2(*c*) and (*d*), forming a step in a low-energy twin interface containing more coincidences (the roof to be switched in this case is orthogonal to the page and parallel to the dense rows). Similarly, flipping corresponds to introducing phason defects in the neighbourhood of the interface. The energetic cost of these defects may be compensated by the increase in coherence of the interface.

DSC vectors are candidates for Burger's vectors of grain boundary dislocations, which accommodate deviations from CSL disorientations. As the physical and perpendicular component of the Burger's vector produces elastic strain and atomic rearrangements (phason strains), respectively, the choice of a particular Burger's vector will depend on the relative energy required to produce physical and phason strains. For the time being, we must appeal to experiment. Recent results for lattice dislocations (Wollgarten, Rosenfeld, Feuerbacher, Metzmacher & Urban, 1995) indicate that a balance is required with phason strain being favoured over physical strain.

To summarize, a grain boundary may seek a minimum of energy by relaxing *via* a series of DSC dislocations minimizing their total free energy by a balance of entropy, phason and physical strain. The boundary plane may also deviate and seek out dense planes of coincident points *via* roof switching and finally by a flipping of vertices an increase in coherence may be obtained at the boundary (Radulescu, Warrington & Lück, 1997).

9. Conclusions

We have shown how the concept of coincidence between rotated crystals may be extended to quasicrystals and to the icosahedral structure in particular. The route to determining the coincidences has been demonstrated and data concerning the corresponding CSL's in hyperspace tabulated for the more important values of $\Sigma < 50$.

We have demonstrated how all possible relative rotations for quasicrystals of icosahedral symmetry may be reduced to presentation within a standard rotation tile and have defined the boundaries of that tile in terms of Σ values. The topology and interconnectivity of the rotation tiles allows a geometric determination of the multiplicity of symmetry-equivalent CSL rotations and proves that only the surfaces of the tiles are represented also by 180° rotations (quasirational rotations with $\Sigma <$ 50 are on the surfaces of the tiles and have at least one twin representation). The determination of multiplicity values allows the expected number of CSL relaxed boundaries to be calculated for a random distribution of rotations; the result is that approximately twice the number of such boundaries would exist compared with a random distribution of cubic 3D crystal boundaries.

The density of coincidence sites per unit area of interface and per unit volume of the icosahedral structure are significant and compare with corresponding values for cubic crystals. Different Σ values show different distributions of coincident vertices; diagrams demonstrate that the twin plane of $\Sigma 4$ has a lower density than those for $\Sigma 5$ and $\Sigma 9$ and may explain why it has not been observed. The uneven distribution of coincidences for $\Sigma 5$ and $\Sigma 9$ may lead to faceted $\Sigma 5$ and $\Sigma 9$ interfaces for grain boundaries deviating from the exact twin plane. This is also typical for a variety of Σ values in cubic crystals.

The coincidence quasilattice (the equivalent of the CSL in cubic crystals) is obtained by cut and projection from the 6D CSL, and therefore is not a complete lattice but itself a quasilattice. It may only be approximately maintained by phason changes resulting from relative displacements of the two quasicrystals. It has been shown for eightfold planar quasicrystals (Radulescu & Warrington, 1996) that the coincidences lost by DSC shifts can be recovered by rearrangements of the structure with no local density change (phason flips). Furthermore, we can show that, under favourable circumstances, an increased grain-boundary coherence may occur beyond that expected from analogy with simple cubic crystals. We shall report in another paper (Radulescu, Warrington, & Lück, 1997) how similar mechanisms may be responsible for grain-boundary relaxation in icosahedral quasicrystals.

The authors are grateful for the support of the Deutsche Forschungsgemeinschaft, the Leverhulme Trust, the Deutscher Akademischer Austauschdienst, the Max Planck Society and the University of Paris 6. They would like to thank Dr M. Kléman and the Laboratoire de Minéralogie–Cristallographie (University of Paris 6) where part of this work was begun and Dr M. Duneau who kindly provided the algorithm for building cut and projection Wieringa roofs. One of the authors (OR) is indebted to Dr J. Roth who showed him a mistake appearing in a previous paper (the minimum index for a disorientation not having a twin representation is $\Sigma 124$ and not $\Sigma 209$).

APPENDIX A
Quasicrystalline directions as twin axes

The directions of the form $\sum z_i \mathbf{e}_i^{\parallel}$ in the icosahedral quasicrystal [modulus or quasicrystalline directions (Katz & Duneau, 1986; Radulescu, 1994, 1995; Radulescu & Warrington, 1995)] always contain two incommensurate (irrational length ratio) vectors. The corresponding 6D vectors span a 2D sublattice L_2. There are two types of directions: even directions, for which L_2 contains only vectors with even sum of indices $\sum_{i=1}^{6} z_i$, and odd directions, for which L_2 contains also vectors with odd sum of indices. We showed (Radulescu, 1995) that for 180° rotations $\Sigma = \Omega_2^2/p$, where Ω_2 is the surface of the unit cell of L_2 (see Table 2) and $p = 1$ or $p = 4$ for odd or even rotation axes, respectively. As Ω_2^2 is always of the form $5x^2 - y^2$, $x, y \in Z$, the coincidence ratios are also of this form.

The fact that indices of a vector on a quasicrystalline direction belong to a 2D lattice introduces some arbitrariness of the indices of a quasicrystalline direction. For instance, a twofold symmetry axis of the icosahedron may be indexed with any integer combination of *e.g.* [101000] and [010100] as may be seen by examining its position with respect to the fivefold axes on the stereographic projection (Fig. 1). For a unique choice, it is necessary in general to impose three conditions; for example, we choose successively: (i) a minimum value of the product $|\mathbf{r}^{\parallel}| \times |\mathbf{r}^{\perp}|$, *i.e.* a minimum value of the form $5(\mathbf{r} \cdot \mathbf{r})^2 - (\mathbf{r} \cdot \mathbf{Sr})^2$ [equation (10)]; (ii) a minimum length in 6D, *i.e.* minimum $\mathbf{r} \cdot \mathbf{r}$; (iii) a minimum length of the physical component $|\mathbf{r}^{\parallel}|$, *i.e.* minimum $\mathbf{r} \cdot \mathbf{Sr}$. Thus, the above twofold axis will index as [010100]. After this choice, the parity of the axis is always the parity of the sum of the indices. An unfortunate inevitable consequence of the choice of minimum $|\mathbf{r}^{\parallel}|$ means that the usual 'zone-law' addition of indices is of very limited applicability but this may be only partially restored by using vector descriptions of non minimum length.

The information on L_2 is not lost when considering only one set of indices instead of two sets. One can always recover the second vector in a basis of L_2 by applying to the first set of indices the matrix $\mathbf{S}$ (if the axis is odd) or $(1 + \mathbf{S})/2$ (if the axis is

even). For instance, $[101000] = (1 + \mathbf{S})/2[010100]$, thus $\{[010100], [101000]\}$ is a basis of the lattice L_2 corresponding to a twofold axis in the icosahedron. Along the same lines, orthogonality of axes $\mathbf{r}_1^{\parallel}$ and $\mathbf{r}_2^{\parallel}$ can be expressed as $\mathbf{r}_1 \cdot \mathbf{r}_2 = 0$ and $\mathbf{r}_1 \cdot \mathbf{S}\mathbf{r}_2 = 0$.

References

Baake, M. (1996). In *The Mathematics of Aperiodic Order*, edited by R. V. Moody & J. Patera. Dordrecht: Kluwer. In the press.

Baake, M. & Pleasants, P. A. B. (1995*a*). *Aperiodic '94*, edited by G. Chapuis & W. Paciorek, pp. 25–29. Singapore: World Scientific.

Baake, M. & Pleasants, P. A. B. (1995*b*). *Z. Naturforsch. Teil A*, **50**, 711–717.

Bollmann, W. (1970). *Crystal Defects and Crystalline Interfaces*. Berlin: Springer Verlag.

Bruijn, N. G. de (1981). *K. Ned. Akad. Wet. Proc. Ser. A*, **84**, 39–66. Reprinted (1987) in *The Physics of Quasicrystals*, edited by P. J. Steinhardt & S. Ostlund, pp. 673–700. Singapore: World Scientific.

Coxeter, H. S. M. (1973). *Regular Polytopes*, p. 31. New York: Dover.

Fortes, M. A. (1983). *Acta Cryst.* A**39**, 351–357.

Frank, F. C. (1988). *Metall. Trans.* **19**A, 403–408.

Grimmer, H., Bollmann, W. & Warrington, D. H. (1974). *Acta Cryst.* A**30**, 197–207.

Harker, D. (1978). *Proc. Natl Acad. Sci. USA*, **75**, 5264–5267.

Katz, A. & Duneau, M. (1986). *J. Phys. (Paris)*, **47**, 181–196.

Kléman, M. (1988). *Quasicrystalline Materials*, edited by C. Janot & J. M. Dubois, p. 318. Singapore: World Scientific.

Kramer, P., Papadopoulos, Z. & Zeidler, D. (1991). *Symposium in Science*, Vol. 5, edited by B. Gruber, p. 305. New York: Plenum Press.

Lück, R. (1988). *Quasicrystalline Materials*, edited by C. Janot & J. M. Dubois, pp. 308–317. Singapore: World Scientific.

Pleasants, P. A. B., Baake, M. & Roth, J. (1996). *J. Math. Phys.* **37**, 1029–1058.

Radulescu, O. (1994). Thèse, Université de Paris Sud, France.

Radulescu, O. (1995). *J. Phys. (Paris) I*, **5**, 719–728.

Radulescu, O. & Warrington, D. H. (1995). *Acta Cryst.* A**51**, 335–343.

Radulescu, O. & Warrington, D. H. (1996). *Materials Science Forum*, Vol. 207–209, edited by A. L. Ferro, J. P. Conde & M. A. Fortes, pp.329–332. Aedermansdorf, Switzerland: Transtec Publications.

Radulescu, O., Warrington, D. H. & Lück, R. (1997). In preparation.

Ranganathan, S. (1966). *Acta Cryst.* **21**, 197–199.

Rolley-Le Coz, M., Senechal, M. & Billiet, Y. (1983). *Acta Cryst.* A**39**, 74–76.

Socolar, J. E. S., Lubensky, T. C. & Steinhardt, P. J. (1986). *Phys. Rev. B*, **34**, 3345.

Warrington, D. H. (1993). *Mater. Sci. Forum*, **126–128**, 57–60.

Warrington, D. H. & Boon, M. (1975). *Acta Metall.* **23**, 599–607.

Warrington, D. H. & Buffalini, P. (1971). *Scr. Metall.* **5**, 771–776.

Warrington, D. H. & Lück, R. (1995). *Aperiodic '94*, edited by G. Chapuis & W. Paciorek, pp. 30–34. Singapore: World Scientific.

Wollgarten, M., Rosenfeld, R., Feuerbacher, M., Metzmacher, C. & Urban, K. (1995). In *Proceedings of the 5th International Conference on Quasicrystals, Avignon, France*, edited by C. Janot & R. Mosseri. Singapore: World Scientific.